X International Conference on Computational Methods for Coupled Problems in Science and Engineering
COUPLED PROBLEMS 2023
M. Papadrakakis, B. Schrefler and E. Oñate (Eds)

IMPLEMENTATION AND FORMULATION OF A MULTI-REGION, ELECTROMAGNETIC SOLVER FOR DISCONTINUOUS MEDIA

Alfred E.J. Bogaers[a], Willem Roos[a], Quinn G. Reynolds[b,c] and Johan H. Zietsman[a,d]

[a] Ex Mente Technologies, South Africa
e-mail: alfred.bogaers@ex-mente.co.za, web page: http://www.ex-mente.co.za/

[b] Pyrometallurgy Division, Mintek, South Africa

[c] University of Stellenbosch, South Africa

[d] University of Pretoria, South Africa

Key words: Electromagnetics, phasor harmonics, partitioned solution, discontinuous materials, OpenFOAM, preCICE

Abstract. The formulation and implementation of a finite-volume, multi-region, electromagnetic solver into OpenFOAM, and coupled using preCICE is presented, to enable the solution of electromagnetic problems with large material discontinuities.

1 INTRODUCTION

In this paper we present the formulation and implementation of a multi-region, electromagnetic solver into OpenFOAM, coupled using preCICE [1]. The solver was developed to handle large material discontinuities, which can typically not be handled using traditional, continuous finite-volume based discretisation schemes.

To facilitate solving Maxwell's equations using the finite volume method (FVM), the equations are formulated in terms of Coulomb gauged magnetic vector potentials and scalar electric potentials. Complex, time-harmonic, phasor approximations are introduced to transform the transient Maxwell equations into a set of quasi-steady equations, which account for the time variations introduced by alternating currents. When posed in this form, large material discontinuities result in severe numerical instabilities when solved using standard FVM discretisation schemes.

Across a discontinuous interface, jump conditions exist in both the electric and magnetic potential fields. Beckstein et al. [2] proposed resolving these discontinuities using embedded FVM discretisation schemes, similar to those used in free surface flow modelling. More recently, Saravia [3] presented a multi-region approach, where the discontinuities within the magnetic potential field were treated with appropriate boundary conditions.

In the current work, we extend on the multi-region idea of Saravia [3], by further posing appropriate jump conditions for the electric potential field interacting with time varying magnetic

fields. The jump conditions for both the electric and magnetic potential fields are implemented as Robin transmission conditions using preCICE, and solved using iterative subcycling. The robustness and accuracy of the proposed solution procedure is demonstrated on a number of appropriate numerical test cases.

2 GOVERNING EQUATIONS

Maxwell's equations, describing the flow of current and magnetic fields through a permeable medium is given by [4]

$$\text{Gauss's law} \quad \nabla \cdot \mathbf{D} = \rho, \tag{1}$$
$$\nabla \cdot \mathbf{B} = 0, \tag{2}$$
$$\text{Faraday's law} \quad \nabla \times \mathbf{E} = -\frac{\partial \mathbf{B}}{\partial t}, \tag{3}$$
$$\text{Maxwell-Ampere law} \quad \nabla \times \mathbf{H} = \frac{\partial \mathbf{D}}{\partial t} + \mathbf{J}, \tag{4}$$

where $\mathbf{E}$ and $\mathbf{H}$ are the electric and magnetic field intensities, $\mathbf{D}$ the electric displacement, $\mathbf{B}$ the magnetic flux field, $\mathbf{J}$ the current density and ρ the charge density. In addition to Maxwell's equations, we also have a charge continuity equation, given by

$$\frac{\partial \rho}{\partial t} + \nabla \cdot \mathbf{J} = 0. \tag{5}$$

To close Maxwell's equations requires constitutive relationships between $\mathbf{D}$ and $\mathbf{E}$, and $\mathbf{B}$ and $\mathbf{H}$. Assuming a continuous, linear, permeable material [4],

$$\mathbf{B} = \mu \mathbf{H} = \mu_0 \mu_r \mathbf{H} = \mu_0 (1 - \chi_m) \mathbf{H}, \tag{6}$$

where μ is a given material's magnetic permeability, $\mu_0 = 4\pi \times 10^{-7}$ the permeability through vacuum, μ_r a material's relative magnetic permeability, and χ_m a material's magnetic susceptibility. The relationship in (6) stems from the observation that exposing a permeable media to an external magnetic field aligns the electrons spin, resulting in a macroscopic induced magnetisation, $\mathbf{M}$. The induced magnetisation in turn results in an induced current $\mathbf{J}_m = \nabla \times \mathbf{M}$, which is implicitly accounted for by the relationship in (6). The electric displacement, $\mathbf{D}$ is related to $\mathbf{E}$ [4] by

$$\mathbf{D} = \epsilon \mathbf{E}, \tag{7}$$

where ϵ is a given material's electric permittivity, and finally Ohm's law relates the current density and electric fields [4], given by

$$\mathbf{J} = \sigma \mathbf{E}, \tag{8}$$

where σ is the isotropic, electrical conductivity.

In this paper, we limit our application of Maxwell's equations to low frequencies (in the order of Hz to kHz instead of MHz to GHz). As such, it is safe to neglect charge displacement (i.e. $\frac{\partial \mathbf{D}}{\partial t} \approx 0$), with no charge build up ($\frac{\partial \rho}{\partial t} = \rho \approx 0$) [5], which reduces Maxwell's equations to

$$\text{Gauss's law} \quad \nabla \cdot \mathbf{E} = 0, \tag{9}$$
$$\nabla \cdot \mathbf{B} = 0, \tag{10}$$
$$\text{Faraday's law} \quad \nabla \times \mathbf{E} = -\frac{\partial \mathbf{B}}{\partial t}, \tag{11}$$
$$\text{Maxwell-Ampere law} \quad \nabla \times \mathbf{B} = \mu \mathbf{J}, \tag{12}$$

where the charge continuity equation reduces to

$$\nabla \cdot \mathbf{J} = 0. \tag{13}$$

Solving the partial differential equations, as posed in Eqs. (9)-(12), using the finite-volume method is a non-trivial exercise, especially when applying generalised boundary conditions. To this end, based on the solonoidal character of the magnetic flux field, and Faraday's law, we can introduce a magnetic vector potential field, $\mathbf{A}$, and a scalar electric potential field, V, such that [2, 3, 4]

$$\mathbf{B} = \nabla \times \mathbf{A}, \tag{14}$$

$$\mathbf{E} = -\nabla V - \frac{\partial \mathbf{A}}{\partial t}. \tag{15}$$

Substituting Ohm's law (8) into the continuity equation (13), using the electric scalar potential relationship (15), results in

$$\nabla \cdot (\sigma \nabla V) = -\nabla \sigma \frac{\partial \mathbf{A}}{\partial t}. \tag{16}$$

Eq. (16) is strictly only valid if σ is continuous everywhere within a given domain [2]. To treat potentially large material discontinuities, we propose in this paper using a decoupled multi-region approach, which is further elaborated on in Section 4.

Similarly, inserting the magnetic potential relationship (14) into the Maxwell-Ampere law, leads to the transport equation for the magnetic potential field, $\mathbf{A}$,

$$\nabla \times \nabla \times \mathbf{A} = \mu\sigma \left(-\nabla V - \frac{\partial \mathbf{A}}{\partial t} \right). \tag{17}$$

Using the Laplacian identity, $\nabla \times \nabla \times \mathbf{A} = \nabla(\nabla \cdot \mathbf{A}) - \nabla^2 \mathbf{A}$, and the Coulomb-gauged assumption of $\nabla \cdot \mathbf{A} = 0$, Eq. (17) reduces to

$$\mu\sigma \frac{\partial \mathbf{A}}{\partial t} - \nabla^2 \mathbf{A} = -\mu\sigma \nabla V. \tag{18}$$

2.1 Phasor representation

In many applications, the time-varying aspect of the electric magnetic fields are driven by time-harmonic alternating source currents, typically described by

$$\mathbf{J} = \mathbf{J}_m \cos(\omega t + \theta), \tag{19}$$

where $\mathbf{J}_m$ is the physical amplitude of the current density, ω the case-specific angular frequency and θ the current phase shift. Solving the transient set of equations, for moderate to high frequencies would require solving for very small time steps. To circumvent this, and assuming that all time variations are solely based on the time-harmonic input currents, it is possible to introduce phasor approximations for the fields of interest, transforming the set of transient equations into a set of quasi-steady equations.

The phasor representation, or phasor transform [2], of Eq. (19) can be stated as

$$\begin{aligned} \mathcal{P}\{J_m cos(\omega t + \theta)\} &= \mathbf{J} \\ &= J_m \cos\theta + j J_m \sin\theta \\ &= J_m e^{j\theta} \Rightarrow J_m \underline{/\theta} \end{aligned} \tag{20}$$

where $J_m\cos\theta$ and $J_m\sin\theta$ represent the real, Re, and imaginary, Im, parts.

Similarly, V, $\mathbf{A}$ and $\mathbf{B}$ can be expressed in terms of their phasor transforms

$$V = V_m e^{(i\omega t + i\theta)} = V_{\mathrm{Re}} + iV_{\mathrm{Im}}, \tag{21}$$

$$\mathbf{A} = \mathbf{A}_m e^{(i\omega t + i\theta)} = \mathbf{A}_{\mathrm{Re}} + i\mathbf{A}_{\mathrm{Im}}, \tag{22}$$

$$\mathbf{B} = \mathbf{B}_m e^{(i\omega t + i\theta)} = \mathbf{B}_{\mathrm{Re}} + i\mathbf{B}_{\mathrm{Im}}. \tag{23}$$

Applying the phasor notation to equations (16) and (18) yields a set of equations which are now a function of complex numbers, given by the real, Re, and imaginary, Im, components, such that

$$\nabla \cdot (\sigma \nabla (V_{\mathrm{Re}} + iV_{\mathrm{Im}})) = -\frac{\partial}{\partial t} \nabla \cdot (\sigma (\mathbf{A}_{\mathrm{Re}} + i\mathbf{A}_{\mathrm{Im}})), \tag{24}$$

$$\nabla^2 (\mathbf{A}_{\mathrm{Re}} + i\mathbf{A}_{\mathrm{Im}}), = \mu\sigma \frac{\partial (\mathbf{A}_{\mathrm{Re}} + i\mathbf{A}_{\mathrm{Im}})}{\partial t} + \mu\sigma \nabla (V_{\mathrm{Re}} + iV_{\mathrm{Im}}). \tag{25}$$

Based on distributive properties involving gradient, divergence and curl operators, along with the observation that two complex numbers can only be equal if the real and imaginary parts are equal, i.e.

$$a + jb = c + jd \iff (a = c \text{ and } b = d), \tag{26}$$

the continuity equations (24) and (25), can each be split into independent real and imaginary components such that

$$\nabla \cdot (\sigma \nabla V_{\mathrm{Re}}) = -\frac{\partial}{\partial t} \nabla \cdot (\sigma \mathbf{A}_{\mathrm{Re}}), \tag{27}$$

$$\nabla \cdot (\sigma \nabla V_{\mathrm{Im}}) = -\frac{\partial}{\partial t} \nabla \cdot (\sigma \mathbf{A}_{\mathrm{Im}}), \tag{28}$$

$$\nabla^2 (\mathbf{A}_{\mathrm{Re}}), = \mu\sigma \frac{\partial}{\partial t} (\mathbf{A}_{\mathrm{Re}}) + \mu\sigma \nabla V_{\mathrm{Re}}, \tag{29}$$

$$\nabla^2 (\mathbf{A}_{\mathrm{Im}}) = \mu\sigma \frac{\partial}{\partial t} (\mathbf{A}_{\mathrm{Im}}) + \mu\sigma \nabla V_{\mathrm{Im}}. \tag{30}$$

Furthermore, since a harmonic solution was assumed, the temporal derivatives of $\mathbf{A}$ can be evaluated analytically, where

$$\frac{\partial \mathbf{A}_{\mathrm{Re}}}{\partial t} = -\omega \mathbf{A}_{\mathrm{Im}}, \quad \frac{\partial \mathbf{A}_{\mathrm{Im}}}{\partial t} = \omega \mathbf{A}_{\mathrm{Re}}. \tag{31}$$

Inserting the analytical temporal derivatives into the continuity equations yields the following final, quasi-steady, harmonic, electromagnetic equations

$$\nabla \cdot (\sigma \nabla V_{\mathrm{Re}}) = +\nabla \cdot (\sigma\omega \mathbf{A}_{\mathrm{Im}}), \tag{32}$$

$$\nabla \cdot (\sigma \nabla V_{\mathrm{Im}}) = -\nabla \cdot (\sigma\omega \mathbf{A}_{\mathrm{Re}}), \tag{33}$$

$$\nabla^2 (\mathbf{A}_{\mathrm{Re}}) = -\mu\sigma\omega \mathbf{A}_{\mathrm{Im}} + \mu\sigma \nabla V_{\mathrm{Re}}, \tag{34}$$

$$\nabla^2 (\mathbf{A}_{\mathrm{Im}}) = +\mu\sigma\omega \mathbf{A}_{\mathrm{Re}} + \mu\sigma \nabla V_{\mathrm{Im}}. \tag{35}$$

3 TIME AVERAGED QUANTITIES OF INTEREST

In the numerical test cases to follow (Section 7), we report a number of post-processed quantities, including Lorentz forces and material self-inductance. This section briefly summarises these quantities of interest in terms of the time averaged values stemming from the time-harmonic, phasor approximations.

The current distribution through a domain, induces thermal energy in the form of Joule heating, which can be computed via [2, 4]

$$P = \mathbf{JE} = \frac{|\mathbf{J}|^2}{\sigma}, \tag{36}$$

for which the time-averaged RMS values can be obtained given the sinusoidally varying input current as

$$P_{\text{avg}} = \frac{1}{2\sigma}\left(\mathbf{J}_{\text{Re}}^2 + \mathbf{J}_{\text{Im}}^2\right). \tag{37}$$

The Lorentz-force, induced by the interaction of current and the magnetic field is given by [2, 4]

$$\mathbf{F} = \mathbf{J} \times \mathbf{B}, \tag{38}$$

where the time averaged Lorentz-force can then be defined as

$$\mathbf{F}_{\text{avg}} = \frac{1}{2}\left(\mathbf{J}_{\text{Re}} \times \nabla \times \mathbf{A}_{\text{Re}} + \mathbf{J}_{\text{Im}} \times \nabla \times \mathbf{A}_{\text{Im}}\right). \tag{39}$$

The stored magnetic energy is given by [4]

$$W_m = \frac{1}{2}\int_V \mathbf{B} \cdot \mathbf{H} dV = \frac{1}{2}\int \frac{1}{\mu}\mathbf{B}^2 dV. \tag{40}$$

The stored magnetic energy in turn is related to a material's self inductance, L, and current I via [4, 10]

$$W_m = \frac{1}{2}LI^2. \tag{41}$$

4 PARTITIONED, MULTI-REGION SOLUTION APPROACH

One of the primary issues when solving Maxwell's equations, using continuum numerical solution schemes, arises when dealing with material discontinuities. When solved for using continuous discretisation schemes, large discontinuities lead to poor numerical stability, often leading to non-convergence. When solvable, standard continuous FVM schemes has further been shown to lead to incorrect results [3], by not appropriately accounting for the jump conditions which exist along the discontinuous interface.

In this paper, we propose resolving these jump conditions by using a multi-region, partitioned coupling approach, similar to the partitioned approaches popularised by the recent advances in black-box, partitioned, multiphysics solvers [1].

The domain, containing multiple different material properties, is decomposed into separate regions, where each region then consists of a single, continuous material property. The various regions are then coupled by iteratively transferring appropriate boundary conditions along the shared interfaces.

In the sections to follow, we briefly outline the necessary and sufficient interface compatibility conditions which need to be satisfied, along with a brief overview of the implementation of the interface boundary conditions.

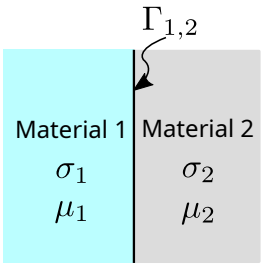

Figure 1: Notional illustration of two magnetic materials sharing a common interface, Γ.

4.1 Magnetic interface compatibility conditions

In this section, the necessary and sufficient, interface compatibility conditions for the electric and magnetic potential fields are presented.

Consider Figure 1, where two magnetic materials, with different material properties, share a common interface Γ. Following on from $\nabla \mathbf{B} = 0$, and the Maxwell-Ampere law, the necessary compatibility conditions, for the magnetic potential field, can be posed as [2, 4, 3]

$$\mathbf{A}_1 = \mathbf{A}_2 \text{ on } \Gamma_{1,2}, \tag{42}$$

and

$$\frac{1}{\mu_1} \cdot \frac{\partial \mathbf{A}_1}{\partial \mathbf{n}} - \frac{1}{\mu_2} \cdot \frac{\partial \mathbf{A}_2}{\partial \mathbf{n}} = \mathbf{K}_f \text{ on } \Gamma_{1,2}, \tag{43}$$

where $\mathbf{K}_f$ is the free surface current. In the current formulation, because the free current is based on Ohm's law ($\mathbf{J} = \sigma \mathbf{E}$), there can be no additional free surface current [4], unless an external user applied surface current is imposed along the shared interface.

Similarly, following from Gauss's law and charge continuity, the compatibility conditions for the electric potential field can be posed as [2, 4]

$$V_1 = V_2 \text{ on } \Gamma_{1,2}, \tag{44}$$

and

$$\mathbf{J}_1 \cdot \mathbf{n}_1 = \mathbf{J}_2 \cdot \mathbf{n}_2 \text{ on } \Gamma_{1,2}, \tag{45}$$

which given the definition of the electric scalar potential (15), results in

$$\sigma_1 \left(\frac{\partial V_1}{\partial \mathbf{n}} + \frac{\partial \mathbf{A}_1}{\partial t} \cdot \mathbf{n}_1 \right) = \sigma_2 \left(\frac{\partial V_2}{\partial \mathbf{n}} + \frac{\partial \mathbf{A}_2}{\partial t} \cdot \mathbf{n}_2 \right) \text{ on } \Gamma_{1,2}. \tag{46}$$

Having assumed the time-harmonic formulation for $\mathbf{A}$ and V, Equations (42), (43), (44) and (46) have to be satisfied for each of the real and imaginary components, leading to the final

necessary and sufficient interface conditions, which have to be satisfied at convergence:

$$\mathbf{A}_{1,\mathrm{Re}} = \mathbf{A}_{2,\mathrm{Re}}, \tag{47}$$

$$\mathbf{A}_{1,\mathrm{Im}} = \mathbf{A}_{2,\mathrm{Im}}, \tag{48}$$

$$V_{1,\mathrm{Re}} = V_{2,\mathrm{Re}}, \tag{49}$$

$$V_{1,\mathrm{Im}} = V_{2,\mathrm{Im}}, \tag{50}$$

$$\frac{1}{\mu_1} \cdot \frac{\partial \mathbf{A}_{1,\mathrm{Re}}}{\partial \mathbf{n}} = \frac{1}{\mu_2} \cdot \frac{\partial \mathbf{A}_{2,\mathrm{Re}}}{\partial \mathbf{n}}, \tag{51}$$

$$\frac{1}{\mu_1} \cdot \frac{\partial \mathbf{A}_{1,\mathrm{Im}}}{\partial \mathbf{n}} = \frac{1}{\mu_2} \cdot \frac{\partial \mathbf{A}_{2,\mathrm{Im}}}{\partial \mathbf{n}}, \tag{52}$$

$$\sigma_1 \frac{\partial V_{1,\mathrm{Re}}}{\partial \mathbf{n}} - \sigma_1 \omega \mathbf{A}_{1,\mathrm{Im}} \cdot \mathbf{n}_1 = \sigma_2 \frac{\partial V_{2,\mathrm{Re}}}{\partial \mathbf{n}} - \sigma_2 \omega \mathbf{A}_{2,\mathrm{Im}} \cdot \mathbf{n}_2, \tag{53}$$

$$\sigma_1 \frac{\partial V_{1,\mathrm{Im}}}{\partial \mathbf{n}} + \sigma_1 \omega \mathbf{A}_{1,\mathrm{Re}} \cdot \mathbf{n}_1 = \sigma_2 \frac{\partial V_{2,\mathrm{Im}}}{\partial \mathbf{n}} + \sigma_2 \omega \mathbf{A}_{2,\mathrm{Re}} \cdot \mathbf{n}_2. \tag{54}$$

4.2 Partitioned coupling interface information transfer

To deal with the large potential material discontinuities using the finite-volume method, we propose using partitioned domain decomposition. Each domain is solved independently, assuming continuous material properties, where information is then iteratively transferred between the various domains sharing a common interface.

To improve stability, and ensure the set of interface compatibility conditions (Eqs. (47)-(54)) are satisfied at convergence, we make use of Robin-Robin interface information transfer, coupled using the preCICE coupling library [1]. To illustrate the implementation of the Robin-Robin interface information transfer, let us consider here the electric potential boundary conditions, reproduced here for clarity:

$$\sigma_1 \left(\frac{\partial V_1}{\partial \mathbf{n}} + \frac{\partial \mathbf{A}_1}{\partial t} \cdot \mathbf{n}_1 \right) = \sigma_2 \left(\frac{\partial V_2}{\partial \mathbf{n}} + \frac{\partial \mathbf{A}_2}{\partial t} \cdot \mathbf{n}_2 \right) \text{ on } \Gamma_{1,2}. \tag{55}$$

To described the surface gradients of the electric potential field, we adopt a similar philosophy as used within the conjugate-heat transfer module of preCICE [6], where

$$\frac{\partial V}{\partial \mathbf{n}} = \frac{V_\Gamma - V_c}{\Delta_x}, \tag{56}$$

where V_Γ is the potential at the boundary, V_c the cell centred value adjoining the boundary cell Γ, and Δ_x the distance from the boundary face to cell centre. Using the gradient approximation, we can rewrite Eq. (55) as

$$\frac{\sigma_{1,\Gamma}}{\Delta_{x,1}}(V_\Gamma - V_{1,c}) + \sigma_{1,\Gamma} \left. \frac{\partial \mathbf{A}_1}{\partial t} \right|_\Gamma \cdot \mathbf{n}_1 = \frac{\sigma_{2,\Gamma}}{\Delta_{x,2}}(V_\Gamma - V_{2,c}) + \sigma_{2,\Gamma} \left. \frac{\partial \mathbf{A}_2}{\partial t} \right|_\Gamma \cdot \mathbf{n}_2. \tag{57}$$

Eq. (57) can then be cast into an OpenFOAM mixed boundary condition, which requires defining the boundary condition in the following form:

$$V_\Gamma = f V_{\mathrm{ref}} + (1 - f)(V_c + \Delta_x g_{\mathrm{ref}}), \tag{58}$$

where f is the value fraction, V_{ref} the potential reference value and g_{ref} the reference gradient. By defininining

$$\alpha_1 = \frac{\sigma_{1,\Gamma}}{\Delta_{x,1}}, \quad \text{and} \quad \alpha_2 = \frac{\sigma_{2,\Gamma}}{\Delta_{x,2}}, \tag{59}$$

and assuming we transfer information from domain 2 to domain 1, the mixed boundary condition coefficients for $V_{\Gamma,1}$, can then be defined as

$$V_{\text{ref}} = V_{2,c} \tag{60}$$

$$f = \frac{\alpha_2}{\alpha_1 + \alpha_2} \tag{61}$$

$$g_{\text{ref}} = \frac{1}{\sigma_{1,\Gamma}} \left(-\sigma_{2,\Gamma} \frac{\partial \mathbf{A}_2}{\partial t} \cdot \mathbf{n}_2 + \sigma_{1,\Gamma} \frac{\partial \mathbf{A}_1}{\partial t} \cdot \mathbf{n}_1 \right). \tag{62}$$

In order to fully define $V_{\Gamma,1,\text{Re}}$ and $V_{\Gamma,1,\text{Im}}$, requires transferring α_2, $V_{2,c,\text{Re}}$, $V_{2,c,\text{Im}}$, $\mu_2\sigma_2\omega\mathbf{A}_{2,\text{Re}}$ and $\mu_2\sigma_2\omega\mathbf{A}_{2,\text{Im}}$ from domain 2 to domain 1. Inversely, for interface information transfer from domain 1 to domain 2 requires transferring α_1, $V_{1,c,\text{Re}}$, $V_{1,c,\text{Im}}$, $\mu_1\sigma_1\omega\mathbf{A}_{1,\text{Re}}$ and $\mu_1\sigma_1\omega\mathbf{A}_{1,\text{Im}}$. The same procedure is employed for the magnetic potential boundaries $A_{\Gamma,1}$ and $A_{\Gamma,2}$ (not shown here for brevity).

For the numerical tests presented in Section 7, preCICE's nearest neighbour interface transfer scheme is used, where the interface meshes are designed to be exactly matching along the various shared interfaces.

5 BOUNDARY CONDITIONS

5.1 Far field boundary

At far field boundaries, Γ_∞, an appropriate boundary condition for the magnetic field is $\mathbf{B} \cdot \mathbf{n}_\infty = 0$, which can be expressed in terms of $\mathbf{A}$, using the Coulomb-gauge condition [2] as

$$\mathbf{n}_\infty \times \mathbf{A} = 0, \quad \text{and} \quad \mathbf{n}_\infty \cdot (\nabla \cdot \mathbf{A}) = 0. \tag{63}$$

Loosely translated, this relates to a boundary condition for $\mathbf{A}$, where the tangential components and normal derivative of $\mathbf{A}$ vanish at Γ_∞.

5.2 Imposed current boundary

To impose a surface current, I, at a boundary, requires defining an electric potential gradient. Using the definition of the electrical potential field (Eq. (15)) and Ohm's law (Eq. (8)), an imposed input current flowing normal through a surface, $\partial\Omega$, is given by

$$\frac{\partial V_{\text{Re,Im}}}{\partial \mathbf{n}} = \frac{I_{\text{Re,Im}}}{\sigma A_{\partial\Omega}} - \frac{\partial \mathbf{A}_{\text{Re,Im}}}{\partial t} \cdot \mathbf{n}, \tag{64}$$

where $A_{\partial\Omega}$ is the surface area, defining the input surface current density (i.e. $\mathbf{J}_{\partial\Omega} \cdot \mathbf{n} = \frac{I_{\partial\Omega}}{A_{\partial\Omega}}$). Based on the time harmonic approximation,

$$I_{\text{Re}} = I_m \cos(\theta) = I_{\text{rms}}\sqrt{2}\cos(\theta), \quad I_{\text{Im}} = I_m \cos(\theta) = I_{\text{rms}}\sqrt{2}\sin(\theta), \tag{65}$$

where θ is the phase shift in the alternating current, I_m the peak magnitude of the alternating input current, and I_{rms} the root mean square of the input current.

6 SEMI-COUPLED MAGNETIC POTENTIAL LINEAR SYSTEM

The partial differential equations describing the time harmonic current and magnetic field distributions (Eqs. (32)-(35)), were implemented in OpenFOAM [7], an open-source, predominantly finite-volume based toolbox, which allows for easy development of continuum based, numerical solvers.

OpenFOAM adopts a staggered solution philosophy, where each equation is solved independently, and any cross-coupling terms in the equations are introduced as explicit source terms. This is especially problematic for the real and imaginary components of $\frac{\partial \mathbf{A}}{\partial t}$, in Eqs. (34) and (35). When σ is large, the magnitudes of the explicit $\mu\sigma\omega\mathbf{A}_{\mathrm{Re}}$ and $\mu\sigma\omega\mathbf{A}_{\mathrm{Im}}$ terms can become several orders of magnitude larger than the implicit divergence terms. In such settings, the convergence of the set of equations is entirely driven by the explicit contributions, which leads to rapid divergence unless very small (in the order of 1×10^{-6}) linear relaxation factors are used.

To improve the overall convergence rates, a partially coupled linear system solution is used, as was first proposed in [2]. The electric potential equations (Eqs. (32) and (33)) are solved in the standard segregated setting, where the two magnetic potential equations are then strongly coupled by solving the linear system

$$\begin{bmatrix} +\mu\sigma\omega & \nabla^2\cdot \\ -\mu\sigma\omega & \nabla^2\cdot \end{bmatrix} \cdot \begin{bmatrix} \mathbf{A}_{\mathrm{Re}} \\ \mathbf{A}_{\mathrm{Im}} \end{bmatrix} = \begin{bmatrix} \mu\sigma\nabla V_{\mathrm{Re}} \\ \mu\sigma\nabla V_{\mathrm{Im}} \end{bmatrix}. \tag{66}$$

The partial coupling is performed using standard OpenFOAM implicit and explicit FV operators, and populating the corresponding matrix coefficients into a larger linear system, solved using the PETSc library [8]. The reason for only partially coupling the two magnetic potential equations, instead of fully coupling all four equations, is that the fully coupled set of equations lead to a poorly conditioned linear system. Numerical experiments have shown that the solution times of the semi-coupled equations, for frequencies in the Hz to kHz range, is several orders faster than solving the full monolithic system. The PETSc implementation is based on the RheoTool collection of libraries and utilities [9].

7 NUMERICAL TESTS

7.1 Copper wire with AC current

In the first test case, we consider an alternating current (AC) source through a copper wire, fully enclosed by air, illustratively shown in Figure 2. When AC travels through a highly conductive medium, the current preferentially travels along the outer periphery of the conductor. This phenomenon is known as the skin effect, where the magnitude and depth of the current along the outer extremities of the conductor is directly proportional to the AC frequency and the magnitude of the electrical conductivity.

The copper wire radius is chosen to be $R = 50\,\mathrm{mm}$, with a length of 0.3m, where the surrounding air is modelled with a radius of 1 m. A time-harmonic AC is imposed at the top of the wire, with $I_{\mathrm{rms}} = 1\,\mathrm{A}$, and a zero potential imposed along the bottom of the wire. The surrounding air boundary conditions are set to be electrically insulating, with $I_{\mathrm{rms}} = 0\,\mathrm{A}$. Since the model is intrinsically symmetrical, the domain is constructed assuming 2D axisymmetry about the central axis.

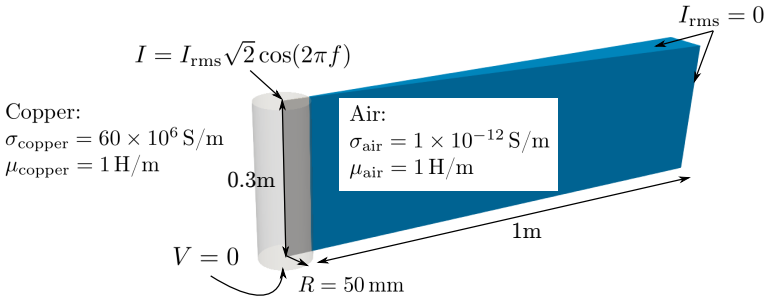

Figure 2: Alternating current through copper conductor test case overview.

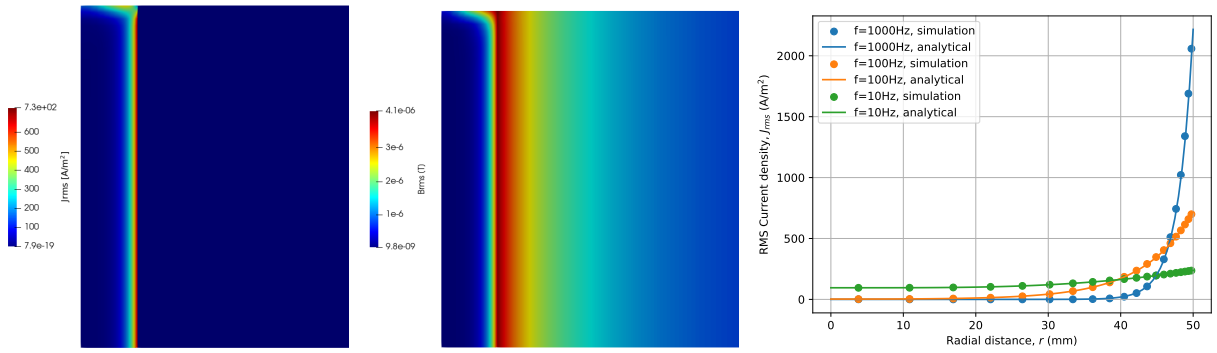

(a) (b) (c)

Figure 3: Copper wire test case results, showing (a) current density and (b) magnetic flux density fields for a frequency of 100 Hz and (c) simulated and analytical current densities for three different frequencies compared to analytical expressions of the current density field.

The current and magnetic flux densities, for a frequency of $f = 100\,\text{Hz}$, is shown in Figure 3. Current uniformly enters the top of the copper conductor, before rapidly concentrating along the conductor's surface. The skin effect is caused by the time varying magnetic field, which induces an electromotive force which the current has to overcome, where the path of least resistance, with the lowest force, is towards the outer extremities of the conductor.

In Figure 3c, the simulated, radially varying current densities, is shown in comparison to analytical expressions. Simulations were performed for three different frequencies of f =10, 100 and 1000 Hz, with a near perfect match to the analytical results. The analytical results, for the radially varying current density, $J(r)$, were computed using [5],

$$J_r = \frac{I(1-i)}{2\pi R\delta}\frac{J_0\left((1-i)r/\delta\right)}{J_1\left((1-i)R/\delta\right)}, \qquad \delta = \sqrt{\frac{2}{\omega\mu\sigma}}, \tag{67}$$

where r is the radial co-ordinate, $J_v(\cdot)$ is the vth order Bessel function of the first kind, and δ is the analytically approximated skin depth.

7.2 Two parallel conductors

In this test case, we model current flowing through two parallel conductors, illustratively shown in Figure 4a. Two 1 m long, copper wires, with radii of $r_w = 4\,\text{mm}$, are separated by a

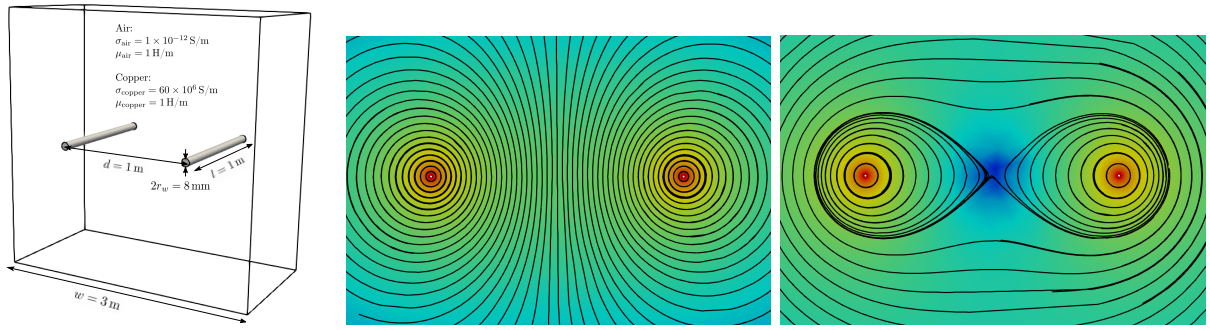

(a) (b) (c)

Figure 4: (a) Two parallel wire test case overview, with magnetic fields lines generated by 1 A flow through the parallel wires, shown for (b) current flowing in opposite directions and (c) current flowing in the same direction.

distance of $d = 1\,\text{m}$. The test case is designed to study the self-inductance and Lorentz forces from the interacting magnetic fields, generated by current flowing through the two wires.

The magnitude of the self generated inductance, for current flowing in opposite directions through two parallel wires, can be approximated using [10]

$$L = \frac{\mu l}{\pi} \ln\left(\frac{d}{r_w} + \frac{1}{4}\right), \tag{68}$$

where the magnitude of the force exerted onto each of the wires, for current in the same direction, can be approximated using [10]

$$F = \frac{\mu I_1 I_2}{2\pi d}. \tag{69}$$

When setting the distance to $d = 1\,\text{m}$, and $I_1 = I_2 = 1\,\text{A}$, results in a force of $2 \times 10^{-7}\,\text{N}m^{-1}$, which is the formal definition of one Ampere.

For the current test case, we apply a DC current to each of the wires, by setting $f = 0\,\text{Hz}$. Two scenarios are tested, the first where a current of 1 A flows through each conductor, in opposite directions (Figure 4b), and the second where a current of 1 A flows in the same direction through each of the wires (Figure 4c). When current flows in the same direction, we expect an attractive force between the two conductors, and an opposing force when the current flows in opposite directions.

In Table 1, we provide a comparison of the the simulated results to the analytical expressions from Eqs. (68)-(69). The model correctly approximates the change in the directionality of the resulting forces, and closely matches the expected impedance and force magnitudes.

7.3 Two parallel conductors with permeable core

In this test case, we demonstrate the ability of the interface conditions to adequetly describe the discontinuity in the magnetic flux field when a magnetic field interacts with a discontinuous permeable material. The test case setup is similar to the parallel conductor case presented in Section 7.2. Two parallel conductors are positioned 1 m apart, each with a radius of 100 mm.

Table 1: Comparison of simulated and analytical impedance and Lorentz force for current flowing through two parallel conductors.

Current		L_{anal}	L_{sim}	$F_{x,\text{anal}}$	$F_{x,\text{sim}}$
I_1[A]	I_2 [A]	(eq. (68)) [H]	[H]	(eq. (69)) [N]	[N]
1	-1	2.31×10^{-6}	2.24×10^{-6}	–	-1.13×10^{-7}
1	1	2.31×10^{-6}	2.70×10^{-6}	2.0×10^{-7}	2.20×10^{-7}

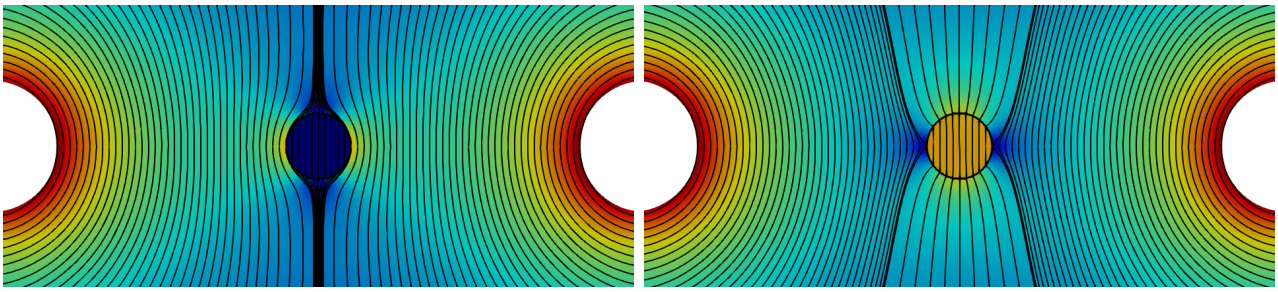

(a) $\mu_r = 1 \times 10^{-3}$ (b) $\mu_r = 1 \times 10^{3}$

Figure 5: Magnetic field lines interacting with permeable core with different relative magnetic permeabilities.

A DC current of 1 A flows in opposite directions, generating a nearly parallel magnetic flux field in the middle of the two conductors. A permeable cylinder, with a radius of 50 mm, is placed in the centre of the magnetic field, where two different relative magnetic permeabilities are tested, namely $\mu_r = 1 \times 10^3$ and 1×10^{-3}, compared to a relative permeability of $\mu_r = 1$ for the surrounding air.

The magnetic flux fields for the two different permeable cores is shown in Figure 5. $\mu_r < 1$ (Figure 5a) represents a diamagnetic material, which repels the magnetic field, leading to a reduction in the magnetic flux field intensity within the diamagnetic core. By contrast, ferromagnetic material, where $\mu_r > 1$ (Figure 5b), attracts the surrounding magnetic field, leading to an increase in the magnetic flux field. In both the diamagnetic and ferromagnetic cases, a jump discontinuity in the magnetic flux field exists across the discontinuous interface.

8 CONCLUSION

In this paper, we presented the formulation and implementation of a multi-region, finite-volume based, electromagnetic solver. The solver was implemented into OpenFOAM, where the various continuous regions were coupled using the preCICE multiphysics coupling library. The solver was designed to handle large material discontinuities, by iteratively transferring the electromagnetic interface jump conditions as Robin-Robin boundary conditions, with iterative subcycling. The validity of the solution procedure was demonstrated on a number of relevant test cases.

REFERENCES

[1] Chourdakis, G. et al., preCICE v2: A sustainable and user-friendly coupling library, *Open Research Europe* (2022).

[2] Beckstein, P., Galindo, V. and Vukcevic, V. Efficient solution of 3D electromagnetic eddy-current problems within the finite volume framework OpenFOAM., *Journal of Computational Physics* (2017).

[3] Saravia, M. A finite volume formulation for magnetostatics of discontinous media within a multi-region OpenFOAM framework. *Journal of Computational Physics* (2021).

[4] Griffiths, D.J., Introduction to electrodynamics, Third Edition, *Prentice Hall* (1999).

[5] Herland, E.V., Sparata, M. and Halversen, S.A., Skin and proximity effects in electrodes and furnace shells, *Metallurgical and Materials Transactions B* (2019).

[6] Yau, L.C., Conjugate heat transfer with the multiphysics coupling library preCICE, Master's Thesis, *Technische Universität München* (2016).

[7] Weller, H.G., Tabor, G. Jasak, H. and Fureby, C., A tensorial approach to computational continuum mechanics using objected-oriented techniques, *Computers in Physics* (1998).

[8] Balay, S., Gropp, W., McInnes, L. C., and Smith, B. F., PETSc, the portable, extensible toolkit for scientific computation, *Argonne National Laboratory* (1998).

[9] Pimenta, F. and Alves, M.A., rheoTool, *https://github.com/fppimenta/rheoTool* (2016).

[10] Wai Kai, C. The electrical engineering handbook, *Elsevier* (2004).